Journal of
Nanoscience and Nanotechnology
Vol. 9, 5795–5802, 2009

Self-Assemblies of Cationic Porphyrins with Functionalized Water-Soluble Single-Walled Carbon Nanotubes

Pavel Kubát[1,*], Kamil Lang[2], Pavel Janda[1], Ota Frank[1,3], Irena Matulková[1], Jan Sýkora[1], Svatopluk Civiš[1], Martin Hof[1], and Ladislav Kavan[1]

[1] *J. Heyrovský Institute of Physical Chemistry, v.v.i., Academy of Sciences of the Czech Republic, Dolejškova 3, 18223 Praha 8, Czech Republic*
[2] *Institute of Inorganic Chemistry, v.v.i., Academy of Sciences of the Czech Republic, 250 68 Řež, Czech Republic*
[3] *Faculty of Science, Charles University, Albertov 6, 128 43, Prague 2, Czech Republic*

5,10,15,20-tetrakis(4-*N*-methylpyridyl)porphyrin, 5,10,15,20-tetrakis(2-*N*-methylpyridyl)porphyrin, and 5,10,15,20-tetrakis(4-trimethylammoniophenyl)porphyrin form self-assemblies with single-walled carbon nanotubes (SWNT) functionalized by polyaminobenzene sulfonic acid. Both steady-state and time-resolved emission studies revealed efficient quenching of the excited singlet states of the porphyrins. Atomic force microscopy, fluorescence confocal microscopy, and fluorescence lifetime imaging allowed the visualization of individual bundles of SWNTs and the differentiation of porphyrin molecules at specific binding sites of SWNT.

Keywords: Cationic Porphyrin, Carbon Nanotubes, Fluorescence Spectroscopy, FTIR, Raman Spectroscopy.

1. INTRODUCTION

Assemblies of single-walled carbon nanotubes (SWNT) with organic chromophores are promising materials for light energy conversion devices due to the unique properties of SWNT, namely, the well-defined electronic and molecular structure, the wide electrochemical stability window, and high surface area.[1,2] The incorporation of light-absorbing antenna chromophores would constitute an ideal system for generating excited states and, thus, the conversion of light to chemical energy. Porphyrins belong to a class of molecules used in donor-acceptor materials in molecular electronics and photovoltaic devices.[3–6]

Several studies have been conducted on the functionalization of SWNT with porphyrin chromophores via non-covalent interactions (nanohybrids)[7–14] and covalent linkages (nanoconjugates).[15–18] The interaction between SWNT and porphyrins led to the formation of supramolecular assemblies that may be followed by a light-induced charge transfer for applications in solar energy conversion. A similar strategy was demonstrated for an assembly of TiO_2/SWNT.[19] Nanohybrids constructed from porphyrin/SWNT are stabilized mainly by π–π interactions between the side walls of SWNT and the porphyrin ring and/or by electrostatic interactions. Recently, complexes of SWNT with other chromophores like sapphyrins,[20] phthalocyanines[21,22] or napthtalocyanines[23] were prepared and their properties have been described.

To harvest the full potential of electrostatic interactions, water-soluble building blocks should be considered because water solubility provides additional flexibility, such as pH variation and ionic strength. Photoexcitation of the porphyrin chromophore can be followed by a rapid and efficient intra-ensemble charge separation, to generate an ion-pair state. The favourable charge-separation features of water-soluble cationic porphyrin/SWNT[7] and pyrene/Zn-porphyrin/SWNT nanohybrids[9] are promising for the construction of photoactive electrode surfaces.

All these considerations led us to investigate the effect of the porphyrin peripheral substitution on the structure and properties of the resulting porphyrin/SWNT nanohybrids. This present contribution is focused on the interaction of porphyrins TMPyP4, TMPyP2, and TMAPP with different cationic substituents and functionalized SWNT in aqueous solutions (Fig. 1). The structure and properties of the resulting complexes were probed by several spectroscopic and microscopic techniques.

*Author to whom correspondence should be addressed.

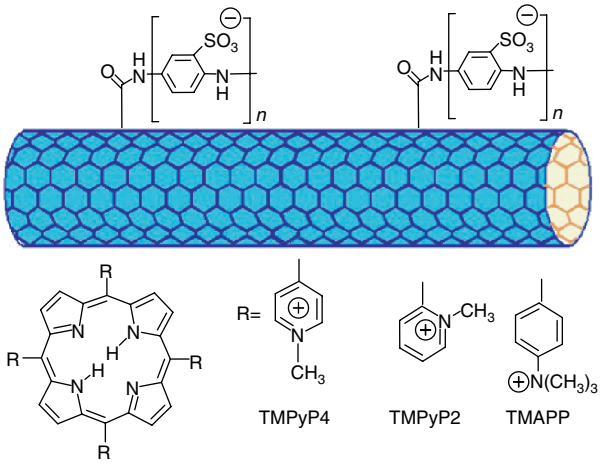

Fig. 1. Structure of the cationic porphyrins and SWNT derivative.

2. EXPERIMENTAL DETAILS

2.1. Materials

The tetratosylate salts of 5,10,15,20-tetrakis(4-*N*-methylpyridyl)porphyrin (TMPyP4, Aldrich), 5,10,15,20-tetrakis(2-*N*-methylpyridyl)porphyrin (TMPyP2, Porphyrin Systems, Germany) and 5,10,15,20-tetrakis(4-trimethylammoniophenyl)porphyrin (TMAPP, Aldrich) were used as received. Single-walled carbon nanotubes (SWNT) functionalized with a water soluble conducting polymer (polyaminobenzene sulfonic acid) covalently bonded to the nanotube core (Aldrich)[24] were dispersed in redistilled water and sonicated for approximately 12 hours until the solution became uniform in colour, indicating good SWNT dispersion.

2.2. Methods and Instrumentation

The steady-state UV/Vis/NIR absorption spectra were measured on a Perkin Elmer Lambda 19 spectrometer. The fluorescence and resonance light-scattering (RLS) spectra were recorded using a Perkin Elmer LS 50B luminescence spectrophotometer. All fluorescence emission spectra were corrected in accordance with the characteristics of the detection monochromator and photomultiplier as described elsewhere.[25] The RLS experiments were conducted using simultaneous scans of the excitation and emission monochromators through the 300–600 nm range. Fluorescence decays were recorded on a 5000U Single Photon Counting setup (IBH, Glasgow, U.K.) using an IBH laser diode NanoLED-440L (440 nm peak wavelength, pulse width < 200 ps, 1 MHz maximum repetition rate) and a cooled Hamamatsu R3809U-50 microchannel plate photomultiplier. Additionally, a 500 nm cutoff filter was used to eliminate scattered light. Data were collected in 2048 channels (52 ps per channel) until the peak value reached 10000 counts. Fluorescence decays were fitted to one- or two-exponential functions using the iterative reconvolution procedure with IBH DAS6 software.

Laser flash photolysis experiments were performed using a Lambda Physik FL 3002 dye laser (425 nm, output 0.05–3 mJ/pulse, pulse width 28 ns).[26] The transient spectra (200–850 nm) were recorded using a laser kinetic spectrometer LKS 20 (Applied Photophysics, UK). The time profiles of the triplet state decays were recorded using a 250 W Xe lamp equipped with a pulse unit, and an R928 photomultiplier (Hamamatsu). The lifetimes of the triplet states (τ_T) were obtained by the fitting of single exponential decay curves in an argon-saturated solution.

The solid structures were prepared by casting a droplet (20–50 μL) of a solution onto the basal plane of a highly ordered graphite (HOPG grade SPI-2, SPI, USA) and mica for AFM measurements, onto quartz substrates for fluorescence microscopy, onto calcium fluoride for FTIR spectroscopy, and onto glass for Raman spectroscopy. The droplet was removed after several minutes and the substrate was dried in ambient air.

FTIR spectra (3940–950 cm^{-1}, spectral resolution of 1 cm^{-1}, 1000 scans) were recorded on a Bruker IFS 120 HR FTIR spectrometer. Micro-Raman analyses were performed on a multichannel Renishaw *In Via* Reflex spectrometer coupled with a Peltier-cooled CCD detector. Excitation was provided either by the 785 nm line of a diode laser or by the 514.5 nm line of an Ar^+ laser. The spectrometer was calibrated against the F_{1g} mode of Si at 520.2 cm^{-1}.

The porphyrin/SWNT self-assemblies were imaged using a tapping and contact mode AFM (Nanoscope IIIa, Veeco, USA). Fluorescence Lifetime Imaging (FLIM) measurements were carried out on an inverted epifluorescence confocal microscope MicroTime 200 (PicoQuant, Germany). We used a configuration containing a pulsed diode laser (LDH-P-C-440, 440 nm, PicoQuant) providing 80 ps pulses at a 40 MHz repetition rate, a proper filter set (clean up filter 440/20, dichroic mirror 505DRLP and long-pass filter LP500 (Omega Optical)), water immersion objective (1.2 NA, 60×) (Olympus), and detector PDM SPAD (MPD, USA). A module Picoharp 300 (PicoQuant, Germany) recorded the photon events in a TTTR mode, enabling the reconstruction of the lifetime histogram for each pixel.[27] A low power of 1.5 μW at the back aperture of the objective was chosen in order to minimize the pile-up effects.

3. RESULTS AND DISCUSSION

3.1. Characterization of SWNT

SWNT were characterized by Vis/NIR absorption spectroscopy, Raman spectroscopy, and by AFM measurements. The latter method shows that the lateral sizes of the nanotube bundles are typically 70–90 nm in the direction parallel to the substrate surface. The vertical sizes of deposited bundles (heights 1.0–2.0 nm) indicate the

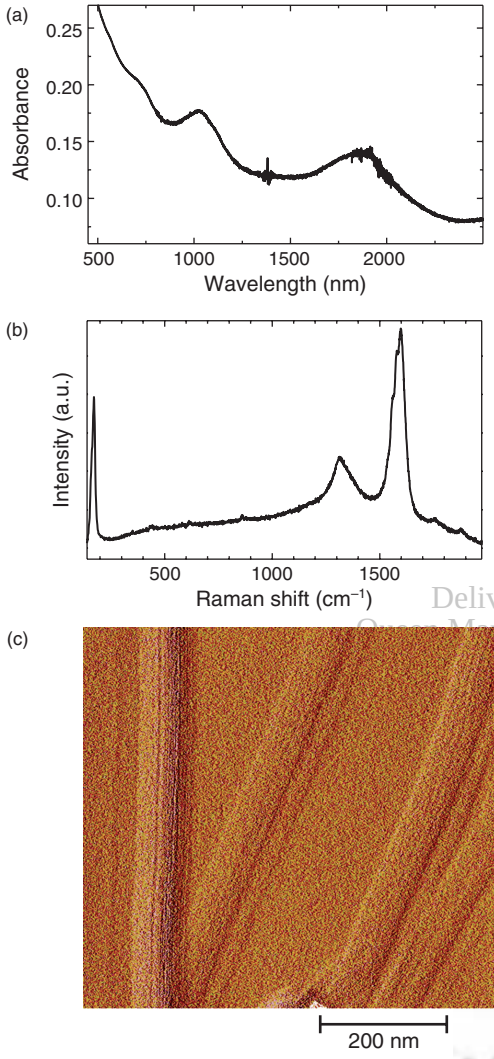

Fig. 2. Vis/NIR spectrum of SWNT (20 mg/L) in D_2O (a), Raman spectrum of SWNT excited by a 785 nm laser line (b), and AFM image of SWNT on an HOPG surface (c).

formation of ribbon-like structures from several nanotubes (Fig. 2(c)).

The Vis/NIR absorption spectrum of SWNT in D_2O (Fig. 2(a)) is dominated by three broad bands centered at 1850, 1050 and 700 nm. These bands correspond to optical transitions between Van Hove singularities in the density of the states of semiconducting nanotubes (1850 and 1050 nm for ΔE_{11}^S and ΔE_{22}^S transitions, respectively) and metallic nanotubes (700 nm for ΔE_{11}^M transition). The mean tube diameter calculated from energy gaps between Van Hove singularities[28] is approximately 1.45 nm.

Figure 2(b) shows the resonant Raman spectrum of pristine SWNT excited by a 785 nm laser. The band at 175 cm^{-1} corresponds to the radial breathing mode (RBM) of SWNT with a diameter of about 1.4 nm.[29] The intensity ratio between the disorder-induced mode (D) around 1320 cm^{-1} and the tangential displacement mode (TG) around 1580 cm^{-1} points to the presence of impurities and/or defects in the SWNT structure.

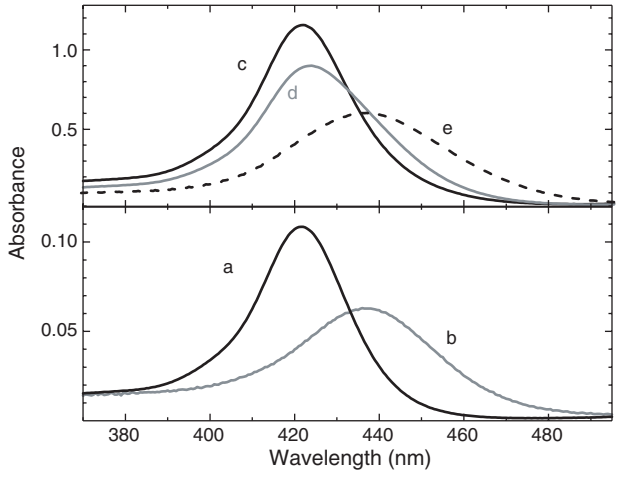

Fig. 3. UV/Vis spectra: TMPyP4 (0.5 μM) before (a) and after addition of SWNT (25 mg/1L) (b); TMPyP4 (6.2 μM) (c), 7 hours (d) and 263 hours after addition of SWNT (e). 20 mM phosphate buffer, pH 7.1, the spectrum of SWNT was subtracted.

3.2. Steady-State UV/VIS Absorption and Fluorescence Spectra

The first insight into the binding of porphyrins to SWNT was obtained by the analysis of UV/Vis spectra. The Soret band of porphyrins is usually very sensitive to external factors such as complexation and aggregation. Porphyrins TMPyP4 (Fig. 3(a)), TMPyP2 and TMAPP show typical monomeric spectra in aqueous solutions with the sharp Soret band ($\varepsilon > 10^5$ M^{-1} cm^{-1}) and four Q-bands at longer wavelengths corresponding to the spectra reported in the literature.[30, 31] The addition of 0.5 μM TMPyP4, TMPyP2, and TMAPP to an aqueous solution of SWNT (25 mg/L) led to a large red shift and hypochromicity of the Soret band (Table I, Fig. 3(b)). The red shift of the Soret band is usually connected with: (i) protonation of the porphyrin ring; (ii) the formation of porphyrin J-aggregates; and (iii) the formation of porphyrin/SWNT self-assemblies.

The protonation of porphyrin pyrrole nitrogens can be excluded at pH 7.1 as the literature values of pK_a are 1.2, 1.8 and 3.0 for TMPyP2, TMPyP4, and TMAPP, respectively.[30] In addition, protonation is accompanied by a decrease in the number of Q-bands to two due to the higher symmetry of porphyrin diacid. However, this change was not observed.

Porphyrin aggregation was investigated by the resonance light scattering technique (RLS), which is a sensitive method for obtaining information about extended aggregates including the absorption spectrum and the average size of the scattering species.[32] The absence of significant RLS signals indicates that porphyrins do not form extended aggregate structures after the addition of SWNT (Figs. 4(a, b)).

Table I. Soret band maxima λ_{max} and photophysical characterization of porphyrin/SWNT self-assemblies: fluorescence lifetimes τ_F, fluorescence quantum yields Φ_F, lifetime of the triplet states τ_T, and rate constant of the triplet states quenching by oxygen k_q. 5 μM porphyrin and SWNT (25 mg/L) in 20 mM phosphate buffer, pH 7.1.

		Fluorescence		Triplet states	
System	λ_{max} (nm)	τ_F (ns)	Φ_F	τ_T (μs)	$10^{-8} \times k_q$
TMPyP4	422	5.1[a] (6.0[b])	(0.086[b])	170	11.8
TMPyP4/SWNT	437	0.87, 5.3[c]	—	162	10.9
TMPyP2	413	14.5[a] (13.8[b])	(0.047[b])	610	9.2
TMPyP2/SWNT	423	1.5, 14.2[c]	—	590	8.9
TMAPP	412	9.3[a] (9.3[d])	(0.070[d])	470	14.0
TMAPP/SWNT	423	0.11, 8.3[c]	—	426	13.4

[a]single exponential decay; [b]Ref. [30]; [c]biexponential decay; [d]Ref. [31].

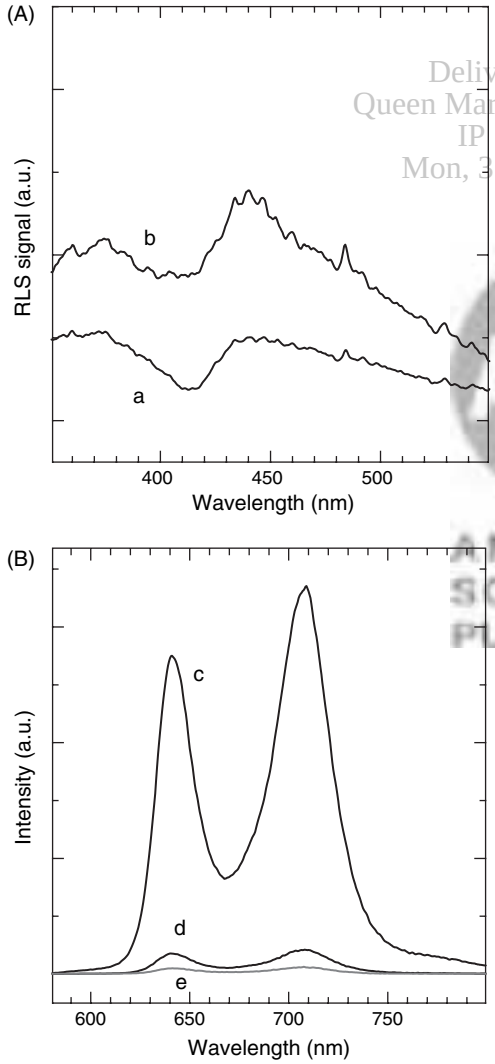

Fig. 4. Panel A: RLS of TMPyP2 (0.8 μM) in the absence (a) and in the presence of SWNT (17 mg/L). The negative peak at 412 nm is due to self-absorption. Panel B: The fluorescence emission spectra of 0.8 μM TMPyP2 (c), after the addition of SWNT (25 mg/L) immediately after mixing (d) and 22 hours after mixing (e). 20 mM phosphate buffer, pH 7.1.

Therefore, the spectral changes can be assigned to the formation of porphyrin/SWNT self-assemblies. The large shift of the Soret bands is comparable with that occurring after intercalation of TMPyP4 between nucleobases of nucleic acids where $\pi-\pi$ interactions between the porphyrin moiety and base pairs play a significant role.[33] We suggest that interaction between porphyrins and SWNT is not based exclusively on electrostatic interactions due to the opposite charges of each component, but on a contribution of $\pi-\pi$ interactions between the porphyrin ring and the walls of SWNT, extensively perturbing the electron configuration of porphyrin, which is reflected by the large shift of the Soret band. TMPyP4/SWNT self-assemblies slowly reorganize over several days as the porphyrin units come into more intimate contact with the SWNT sidewall via $\pi-\pi$ interactions, which is represented by an additional red shift of the Soret band (Figs. 3(d, e)). Similar behaviour was observed for TMPyP2/SWNT and TMAPP/SWNT self-assemblies.

The positions of the bands in fluorescence emission spectra of porphyrin/SWNT self-assemblies are the same as those of free porphyrins (Fig. 4). In contrast, the fluorescence intensities strongly decrease with decreasing porphyrin/SWNT ratios (Fig. 4(c, d)) and with ageing (Fig. 4(e)). The general behaviour can be demonstrated on the TMPyP2/SWNT system. The fluorescence excitation spectra do not mirror the changes in the ground state absorption spectra after the addition of SWNT. However, the spectra are consistent with those of TMPyP2 itself (Fig. (5)). The behaviour can be explained by two limited porphyrin forms: fluorescent unbound porphyrin molecules and non-fluorescent porphyrins attached to SWNT.

3.3. Time-Resolved Measurements

The fluorescence decays of the studied porphyrins are mono-exponential with the lifetimes comparable with literature data (Table I). In the presence of SWNT the decays become bi-exponential with the long-lived component belonging to unbound porphyrin and the increasing contribution of a short-lived component as the porphyrin/SWNT ratio decreases. As with the quenching of fluorescence

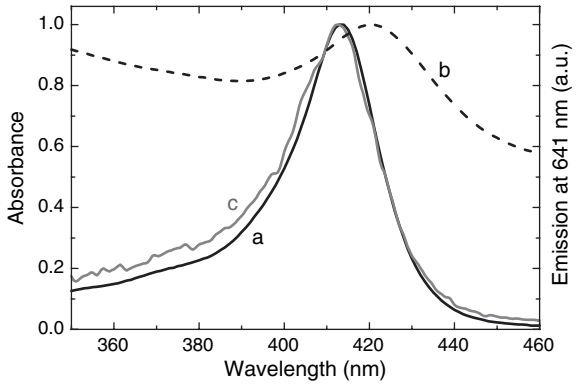

Fig. 5. Comparison of the normalized absorption spectra of (a) TMPyP2 (0.8 μM), (b) TMPyP2 (0.8 μM) and SWNT (17 mg/l), (c) excitation spectra of TMPyP2 and SWNT (right axis). 20 mM phosphate buffer, pH 7.1.

emission spectra, this behaviour can be attributed to deactivation of the S_1 states within the porphyrin/SWNT self-assembly. The absence of fluorescence upon binding to SWNT indicates a new deactivation pathway. As the pulse width of the laser diode used for excitation is about 200 ps, we cannot exclude the contribution of a faster decay process.

In order to explore the effect of SWNT on the triplet-state dynamics of the porphyrin moieties, we carried out nanosecond laser flash photolysis measurements. The difference absorption spectra of TMPyP2, TMPyP4 and TMAPP measured after excitation into the corresponding Soret bands consisted of the broad triplet–triplet absorption bands with maxima at 460 nm.[34] The triplet states are quenched by oxygen according to the first-order kinetics and the lifetimes in argon-saturated solutions (τ_T) are of 610, 170 and 470 μs for TMPyP2, TMPyP4, and TMAPP, respectively (Table I). The addition of SWNT considerably decreases the amplitudes of the triplet states and has a minor effect on the triplet lifetimes τ_T. It indicates that the triplet states of unbound porphyrins were generated.

Individual SWNT and bundles of different sizes and chirality can exhibit different electrochemical behaviour. We assume that the conduction band edge of semiconducting SWNT is in the range of -0.5 to 1 V versus a normal hydrogen electrode (NHE)[35] and that the oxidation potential of the TMPyP4 pair ($TMPyP4^+$/TMPyP4) is 1.30 V versus NHE.[36] Taking into account the excitation energy of the singlet states (1.83 eV for TMPyP4), this confirms that the mechanism of singlet-state quenching is likely to involve a thermodynamically favourable electron transfer from the porphyrin moiety into SWNT. The triplet states of TMPyP4 (excitation energy 1.44 eV) probably do not play a major role in the photoinduced electron transfer because the triplet lifetime is only slightly reduced in the presence of SWNT (Table I). Similar estimations cannot be performed for TMPyP2 and TMAPP since their oxidation potentials are not reported in the literature.

We have not found any spectroscopic evidence for the existence of radical ions in TMPyP4, TMPyP2, and TMAPP/SWNT systems by nanosecond laser flash photolysis experiments. Nevertheless, a charge transfer process without complete charge separation may occur on the femtosecond–picosecond timescale. The literature data for similar systems show that excitation of the supramolecular self-assembly of Zn porphyrin with SWNT functionalized by pyridinium groups does not lead to electron transfer with the generation of charge-separated states.[37] On the other hand, photoinduced charge separation and ion-pair lifetimes on the range of microseconds have been described for other porphyrin/SWNT nanohybrids.[7, 8]

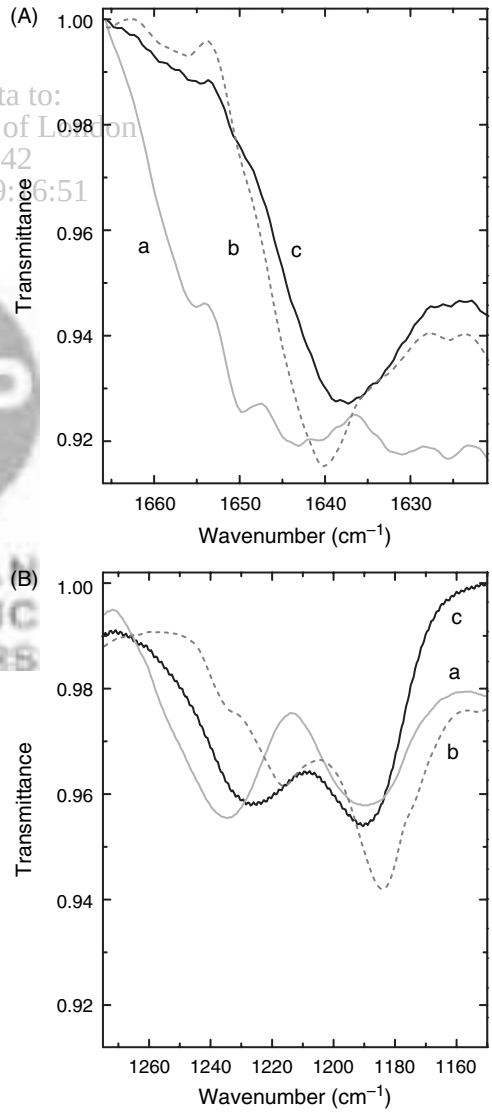

Fig. 6. FTIR spectra of the solid films prepared by the drop-casting of an aqueous solution of SWNT (17 mg/l) (a), 6.2 μM TMPyP4 (b) and 6.2 μM TMPyP4/SWNT (17 mg/L) self-assembly (c) onto CaF_2 window. Panel A shows the 1660–1620 cm^{-1} region and Panel B the 1275–1150 cm^{-1} region.

3.4. Vibrational Spectroscopy

Additional information on porphyrin/SWNT self-assemblies is deduced from FTIR and Raman spectra. FTIR spectra of solid films prepared by the drop-casting of aqueous solutions of a SWNT (Fig. 6(a)), TMPyP4 (Fig. 6(b)) and TMPyP4/SWNT mixture (Fig. 6(c)) onto a CaF_2 window prove a strong electrostatic interaction between SO_3^- groups of SWNT and positively charged porphyrin substituents. Several noteworthy features can be observed in the 1260–1160 cm^{-1} and 1660–1625 cm^{-1} regions.

Two medium broad bands in the spectral region 1260–1160 cm^{-1} identified as a stretching vibration of the SO_3^- group[38] originate from SWNT (1235 and 1189 cm^{-1}, Fig. 6(a)). The band at 1216 cm^{-1} and the shoulder at 1232 cm^{-1} correspond to the deformation of *N*-methylpyridyl and the band at 1184 cm^{-1} can be assigned to the mixture of deformation and stretching vibrations of *N*-methylpyridyl and N^+-CH_3 (Fig. 6(b)),[39] respectively. Although the bands of *N*-methylpyridyl and SO_3^- groups are partially overlapped, it is clearly seen that the FTIR spectrum of the TMPyP4/SWNT self-assembly (Fig. 6(c)) is not a simple superposition of the spectra of both components.

The narrow band of deformation vibration of the *N*-methylpyridyl group[40] in the spectrum of TMPyP4/SWNT is shifted to 1638 cm^{-1} and extended due to the carbonyl stretch of SWNT amide. For comparison, free TMPyP4 displays this band at 1640 cm^{-1}. The above mentioned broad band at 1643 cm^{-1} assigned to the amide carbonyl stretch is observed in the FTIR spectrum of SWNT (Fig. 6(a)). A similar shift was found for the

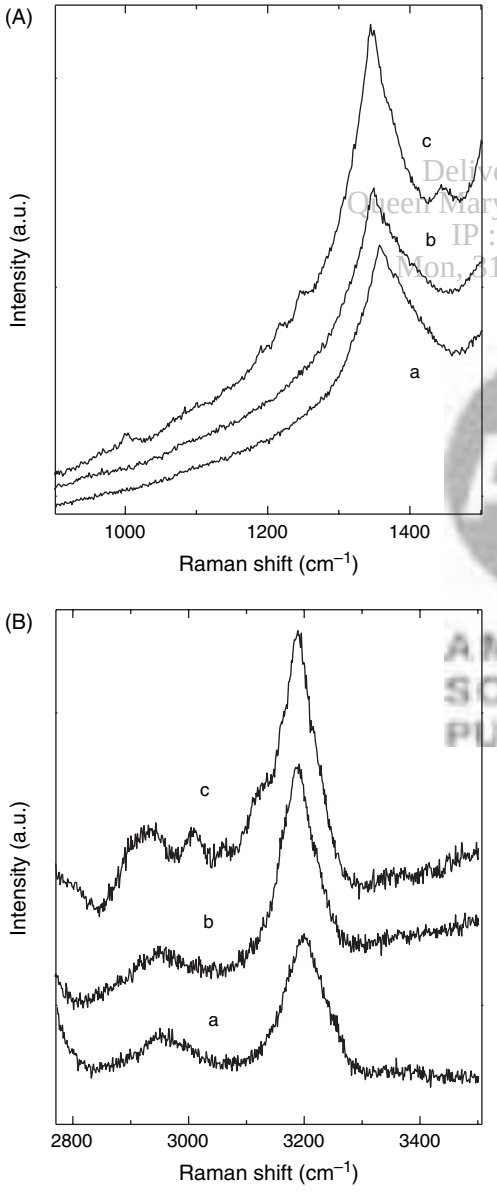

Fig. 7. Raman spectra of SWNT as received (a), SWNT drop-cast onto a glass slide (b), TMPyP4/SWNT self-assembly drop-cast onto a glass-slide (c). Panel A shows the 900–1500 cm^{-1} and Panel B the 2750–3500 cm^{-1} regions, the spectra are normalized to the G-band intensity.

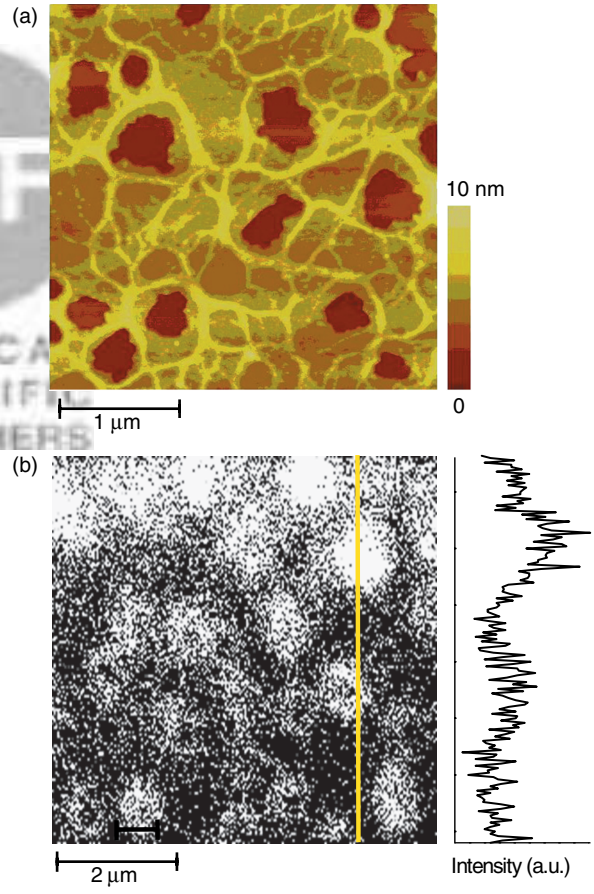

Fig. 8. Tapping mode AFM (a) and fluorescence intensity (b) images of the TMPyP4/SWNT self-assembly. The samples were prepared by drop-casting from an aqueous solution containing SWNT (12 mg/L) and 2 μM TMPyP4 (incubation time of 72 hours). The intensity profiles are on the right of the figure.

coulombic interaction between Ni salt of TMPyP4 and DNA.[41]

The Raman spectra of pristine SWNT (Fig. 7(a)) and SWNT drop-cast onto a glass slide from an aqueous solution (Fig. 7(b)) have the same characteristic bands which vary slightly in intensity due to the different background signals. However, additional minor peaks appear in the spectrum of the TMPyP4/SWNT self-assembly (Fig. 7(c)) in the regions 1000–1300 cm^{-1} and 2800–3200 cm^{-1} and around 1450 cm^{-1}. The spectra of free porphyrins were not measured because of their strong fluorescence background. The spectra in panel A are, as expected, dominated by the D-band of SWNT. The peak at 1000 cm^{-1} can be tentatively assigned to a ring deformation vibration (e.g., of pyridine), the peaks between 1200–1260 cm^{-1} to C–H deformation vibrations, and the peak at 1500 cm^{-1} to C=N or C=C in plane vibration (Fig. 7, panel A). In the second spectral region (Fig. 7, panel B), symmetric and antisymmetric methyl group stretching vibrations could be assigned to the peaks around 2900 and 3000 cm^{-1}, and the C–H stretching modes of aromatic systems assigned to the peaks around 3100 cm^{-1}.[42] We assume that these peaks originate from the bound porphyrin moiety.

3.5. Characterization of Porphyrin/SWNT Self-Assemblies on Solid Substrates by Microscopic Techniques

When SWNT are transferred to a substrate, bundles consisting of several nanotubes are formed (Fig. 2(c)). Figure 8(a) shows a random SWNT network which is surrounded by a lower layer of porphyrin molecules bound to the side chains. The presence of porphyrins can make peripheral hydrophilic polyaminobenzene sulfonate side chains visible.

The fluorescence intensity image of these structures shows similar patterns (Fig. 8(b)). The higher-intensity spots can be interpreted as the fluorescence of porphyrins bound to the side chains of SWNT, but not in intimate contact with the nanotube core. The dark sites contain non-fluorescent porphyrin molecules which are efficiently quenched by nanotube and/or do not contain any porphyrin molecules. Note that the diffraction limited spatial resolution of confocal fluorescence microscopy is about 200 nm and that it is much worse than that of AFM measurements.

The intensity image of the individual TMPyP4/SWNT structure obtained at higher TMPyP4 concentration is shown in Figure 9(a). The corresponding intensity decay curves from each pixel were analyzed by a three-exponential function resulting in a lifetime equal to the time resolution of the experiment ($\tau_1 = 200$ ps) and two nanosecond components ($\tau_2 = 700$ ps and $\tau_3 = 3.5$ ns, respectively). Since the first component is missing in the bulk experiments (Table I), it is probably due to light scattering. Figure 9(b), which shows the relative amplitudes of that component, is qualitatively similar to Figure 9(a), thus indicating that the majority of recorded photons is indeed due to light scattering. Figure 9(c) shows the amplitude image of the true fluorescence component $\tau_2 = 700$ ps. It appears that TMPyP4 is homogeneously distributed within the SWNT bundles. The same conclusion can be drawn for the amplitude image of the second fluorescence component (data not shown).

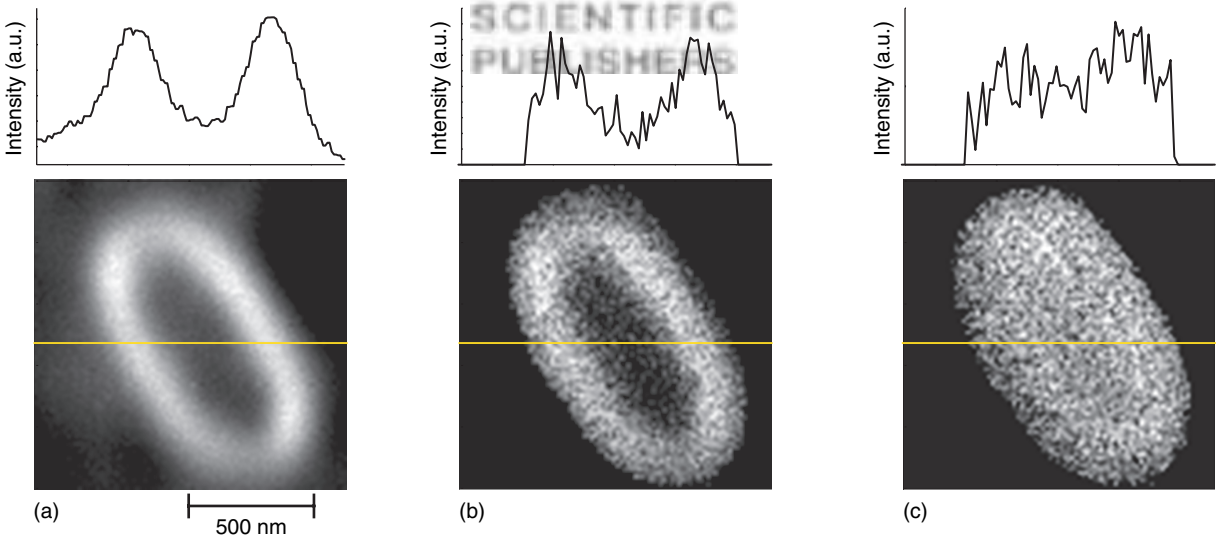

Fig. 9. Fluorescence intensity image of the individual structure formed from TMPyP4 and SWNT on a glass substrate (a) and images constructed from amplitudes of individual components of three-exponential decay: component with $\tau_1 = 200$ ps assigned to light scattering (b) and fluorescence decay with $\tau_2 = 700$ ps (c). The upper graphs show fluorescence intensities along the marked line. The sample was prepared by drop-casting from an aqueous solution of SWNT (12 mg/L) and 25 μM TMPyP4 (incubation time of 2 hours).

4. CONCLUSION

We have designed new water-soluble porphyrin/SWNT nanohybrids. Their properties were studied by steady-state and time-resolved spectroscopy techniques as well as by atomic force and fluorescence microscopy. Strong fluorescence quenching and a free energy calculation based on the electrochemical redox data revealed the possibility of photoinduced electron transfer from the porphyrin moiety to SWNT. In constrast to previously published similar systems based on coloumbic attraction between peripheral substituents,[7] the formation of corresponding ion pairs was not confirmed by the transient absorption measurement on the nanosecond time scale.

Acknowledgments: This research was supported by the Czech Science Foundation (Nos. 203/07/1424 and 203/06/1244), by the Academy of Sciences of the Czech Republic (Nos. KAN100500652, IAA400400804 and KAN200100801) and by the Ministry of Education, Youth and Sports of the Czech Republic (No. LC-510).

References and Notes

1. D. M. Guldi, *Nature* 447, 50 (**2007**).
2. L. Kavan and D. Dunsch, *ChemPhysChem* 8, 974. (**2007**).
3. D. Ren, Z. Guo, F. Du, J. Zheng, and Y. Chen, *J.Nanosci. Nanotechnol.* 7, 1539 (**2007**).
4. D. S Hecht, R. J. A. Ramirez, M. Briman, E. Artukovic, K. S. Chichak, J. F. Stoddart, and G. Gruner, *Nano Letters* 6, 2031 (**2006**).
5. S. Takagi, M. Eguchi, D. A. Tryk, and H. Inoue, *J. Photochem. Photobiol. C* 7, 104 (**2006**).
6. D. A. Britz and A. N. Khlobystov, *Chem. Soc. Rev.* 35, 637 (**2006**).
7. D. M. Guldi, G. M. Rahman, J. Ramey, M. Marcaccio, D. Paolucci, F. Paolucci, S. Qin, W. T. Ford, D. N. Balbinot, N. Jux, N. Tagmatarchis, and M. Prato, *Chem. Commun.* 2034 (**2004**).
8. K. Saito, V. Troiani, H. Qiu, N. Solladie, T. Sakata, H. Mori, M. Ohama, and S. Fukuzumi, *J. Phys. Chem. C* 111, 1194 (**2007**).
9. C. Ehli, G. M. Rahman, N. D. JuxBalbinot, D. M. Guldi, F. Paolucci, M. Maraccio, D. Paolucci, M. Melle-Franco, F. Zerbetto, S. Campidelli, and M. Prato, *J. Am. Chem. Soc.* 128, 11222 (**2006**).
10. A. Satake, Y. Miyajima, and Y. Kobuke, *Chem. Mater.* 17, 716 (**2005**).
11. T. Hasobe, S. Fukuzumi, and P. V. Kamat, *J. Phys. Chem. B* 110, 25477 (**2006**).
12. K. Saito, V. Troiani, H. Qiu, N. Solladie, T. Sakata, H. Mori, M. Ohama, and S. Fukuzumi, *J. Phys. Chem. C* 111, 1194 (**2007**).
13. D. R. Kauffman, O. Kuzmych, and A. Star *J. Phys. Chem. C* 111, 3539 (**2007**).
14. F. D'Souza, R. Chitta, A. S. D. Sandanayaka, N. K. Subbaiyan, L. D'Souza, Y. Araki, and O. Ito, *Chem-Eur. J.* 13, 8277 (**2007**).
15. T. Umeyama, M. Fujita, N. Tezuka N. Kadota, Y. Matano, K. Yoshida, S. Isoda, and H. Imahori, *J. Phys. Chem. C* 111, 11484 (**2007**).
16. S. Campidelli, C. Sooambar, E. L. Diz, C. Ehli, D. M. Guldi, and M. Prato, *J. Am. Chem. Soc.* 128, 12544 (**2006**).
17. C. Ehli, S. Campidelli, F. G. Brunetti, M. Prato, and D. M. Guldi, *J. Porph. Phthal.* 11, 442 (**2007**).
18. Z. Guo, F. Du, D.M. Ren, Y. Chen, J. Zheng, and Z. J. Liu Tian, *J. Mater. Chem.* 16, 3021 (**2006**).
19. A. Kongkanand and P. V. Kamat, *ACSNano* 1, 13 (**2007**).
20. P. J. Boul, D. G. Cho, G. M. Rahman, M. Marquez, Z. Ou, K. M. Kadish, D. M. Guldi, and J. L. Sessler, *J. Amer. Chem. Soc.* 129, 5683 (**2007**).
21. Q. Y. Liu, Y. Li, H. G. Liu, Y. L. Chen, X. Y. Wang, Y. X. Zhang, X. Y. Li, and J. Z. Jiang, *J. Phys. Chem. C* 111, 7298 (**2007**).
22. B. Ballesteros, G. de la Torre, C. Ehli, G. M. Rahman, F. Agullo-Rueda, D. M. Guldi, and T. Torres, *J. Amer. Chem. Soc.* 129, 5061 (**2007**).
23. R. Chitta, A. S. D. Sandanayaka, A. L. Schumacher, L. D'Souza, Y. Araki, O. Ito, and F. D'Souza, *J. Phys. Chem. C* 111, 6947 (**2007**).
24. M. E. Itkis, D. E. Perea, S. Niyogi, S. M. Rickard, M. A. Hamon, H. Hu, B. Zhao, and R. C. Haddon, *Nano Letters* 3, 309 (**2003**).
25. J. A. Gardecki and M. Maroncelli, *Appl. Spectrosc.* 52, 1179 (**1998**).
26. P. Kubát, K. Lang, P. Cígler, M. Kožíšek, P. Matějíček, P. Janda, Z. Zelinger, K. Procházka, and V. Král, *J. Phys. Chem. B* 111, 4539 (**2007**).
27. P. Kapusta, M. Wahl, A. Benda, M. Hof, and J. Enderlein, *J. Fluoresc.* 17, 43 (**2007**).
28. M. S. Dresselhaus, G. Dresselhaus, and P. C. Eklund, Science of Fullerenes and Carbon Nanotubes, Academic Press, San Diego (**1996**).
29. M. S. Dresselhaus, G. Dresselhaus, R. Saito, and A. Jorio, *Phys. Reports* 409, 47 (**2005**).
30. K. Kalyanasundaram, *Inorg. Chem.* 23, 2453 (**1984**).
31. K. Kalyanasundaram, *J. Chem. Soc., Faraday Trans. 2* 79, 1365 (**1983**).
32. R. F. Pasternack and P. J. Collings, *Science* 369, 935 (**1995**).
33. N. E. Mukundan, G. Petho, D. W. Dixon, M. S. Kim, and L. G. Marzilli, *Inorg. Chem.* 33, 4676 (**1994**).
34. P. Kubát, K. Lang, P. Lhoták, P. Janda, P. Matějíček, J. Sýkora, M. Hof, K. Procházka, and Z. Zelinger, *J. Photochem. Photobiol A* 198, 18 (**2008**).
35. M. J. O'Connell, E. E. Eibergen, and S. K. Doorn, *Nature Mat.* 4, 412 (**2005**).
36. K. Kalyanasundaram and M. Neumann-Spallart, *J. Phys. Chem.* 86, 2681 (**1982**).
37. M. Alvaro, P. Atienzar, P. de la Cruz, J. L. Delgado, V. Troiani, H. Garcia, F. Langa, A. Palkar, and L. Echegoyen, *J. Amer. Chem. Soc.* 128, 6626 (**2006**).
38. L. Ganguly, C. I. Jose, and A. B Biswas, *Spectrochim. Acta A* 24 215 (**1968**).
39. S. Rywkin, C. M. Hosten, J. R. Lombardi, and R. L. Brike, *Langmuir* 18, 5869 (**2002**).
40. G. Miguel, M. Pérez-Morales, M. T. Martín-Romero, E. Munoz, T. H. Richardson, and L. Camacho, *Langmuir* 23, 3794 (**2007**).
41. Y. Nonaka, S. D. Lu, A. Dwivedi, P. D. Storommen, and K. Nakamoto, *Biopolymers* 29, 999 (**1990**).
42. G. Socrates, Infrared and Raman Characteristic Group Frequencies. Tables and Charts, John Wiley, New York (**2001**).

Received: 1 September 2008. Accepted: 2 November 2008.